Journal of Materials Chemistry B

Accepted Manuscript

ROYAL SOCIETY OF CHEMISTRY

www.rsc.org/materialsB

Journal of
Materials Chemistry B

RSCPublishing

PAPER

A Photoacoustic Approach for Monitoring the Drug Release of pH-sensitive Poly(*β*-amino ester)s

Cite this: DOI: 10.1039/x0xx00000x

Zhongyu Duan *[a], Yujuan Gao [ab], Zengying Qiao [b], Gang Fan [b], Ya Liu [b], Di Zhang [b], Hao Wang *[b]

Received 00th January 2014,
Accepted 00th January 2014

DOI: 10.1039/x0xx00000x

www.rsc.org/

Drug delivery systems are capable of delivering medications to target sites and controlled releasing payloads to circumvent common problems associated with traditional drugs such as low bioavailability and undesired side-effects. Real-time and spatio-temporal monitor of the drug release kinetics is crucial for evaluating treatment efficacy. The photoacoustic tomography (PAT) imaging technique becomes an emerging tool for non-invasively studying the drug release behaviour from drug-loaded nanocarriers in physiological conditions. In this work, we prepared PEG modified poly(*β*-amino ester)s graft copolymers with pH-sensitive property, which were proved by pyrene fluorescence and pH titration measurements. The copolymers could form micelle-like nanoparticles with hydrophobic cores at pH 7.4 and dissociated into single chains in mildly acidic media. The anticancer drug doxorubicin (DOX) and near-infrared fluorescence squaraine (SQ) dye as a built-in PAT reporter molecule were loaded into the hydrophobic core of micelles simultaneously, and their release profiles were investigated by UV-Vis, fluorescence spectrometers and PAT technique. The polymer micelles were stable at pH 7.4 and released the loaded molecules quickly at mildly acidic condition, accompanied by the change of photoacoustic signals. The drug-loaded micelles entered into human breast cancer MCF-7 cells by endocytosis and accumulated in the lysosomes that provide an acidic environment to promote the release of DOX, which were monitored by PAT imaging. The time-dependent photoacoustic signals in tissue-mimic phantoms containing micelle-like nanoparticles treated cells reflected the drug release process in lysosomes, which was further validated by cell-based confocal fluorescence microscope.

Introduction

In the past several decades, smart polymers have attracted great interests due to their broad applications in both nanotechnology and biomedicine.[1-4] Among them, stimuli responsive polymers have been extensively studied as drug nanocarriers, which have many advantages over liposomes, including high stability, long circulation time in bloodstream, good mechanical property, and advanced chemical modification.[5-10] These polymeric nanocarriers show great potentials for accumulating at tumor sites *via* enhanced permeability and retention (EPR) effect and decreasing the systemic toxicity.[11-13] The controlled release behaviours of anticancer drugs from nanocarriers play a vital role in enhancing cancer treatment efficacy.[14-16] Although the drug release profiles and kinetics have been studied widely in aqueous solution,[17, 18] the drug release behaviours in cellular or tissue level are more important but less investigated owing to the intrinsic technique limitation of the conventional semi-quantitative fluorescence method.[19-21]

Recently, photoacoustic tomography (PAT) technique has been developed rapidly in biology for organelles, cells, tissues, and organs imaging.[22-24] As a promising biomedical diagnostic tool, PAT imaging exhibits the high spatial resolution and deep tissues penetration capability. Various nanomaterials have been applied as contrast agents for *in vivo* tumor PAT imaging, such as nanotubes/ graphene oxide,[25-27] gold nanoparticles [28, 29] and near-infrared (NIR) fluorescent dyes,[30-33] etc. The biomolecules around contrast agents absorb photons thermoelastically inducing pressure waves by the photoacoustic effect, generating ultrasonic waves, which are detected and calculated to form PAT images. Squaraine dyes are one of the most interesting NIR fluorescent dyes with high absorption co-efficiency, bright fluorescence and good photostability.[34, 35] Squaraine dye-based macrocyclic rotaxanes with high stability have been applied for bioimaging.[36-42] Würthner *et al.* have developed a series of dicyanovinyl-functionalized squaraine dyes, which show superior NIR fluorescence properties and high chemical stability.[34, 39, 43-45] The hydrophobic NIR dyes can be capsulated in nanocarriers such as BSA for fluorescence imaging.[46]

The pH-sensitive polymers have been developed widely as anticancer drug carriers due to the weakly acidic environment in the intracellular compartments such as endosomes and lysosomes (pH = 5.0–6.0),[47-49] including polymers with tertiary amine groups,[50-52] acetals/ketals,[53-56] ortho esters,[57-63] hydrazine/imide bonds,[64-69] etc. Langer et al. have developed a series of poly(*β*-amino ester)s as gene/drug carriers by Michael addition,[70-74] which have tertiary

amine groups with a pK_b value around 6.5. Other groups also reported PEG modified poly(*β*-amino ester)s with various structures, which could load anticancer drugs and released them in acidic media.[19-21] We have prepared poly(RGD-*co*-*β*-amino ester) copolymers through the simple, reliable and one-pot synthesis method, which have enhanced killing efficacy towards U87 cells.[75] However, one of unsolved problems is how to quantitatively evaluate the drug release profile from polymer carriers in biological environment.

In this study, we first utilized PAT imaging to monitor the drug release behaviours from pH-sensitive polymer carriers. The graft polymers poly(*β*-amino ester)s (**P1** and **P2**) with PEG side chains were synthesized by Michael addition, which were further self-assembled into micelle-like nanoparticles at neutral pH. At the same time, the anticancer drug (DOX) and the built-in NIR fluorescence dye SQ were loaded into the hydrophobic core of polymer micelles (**Scheme 1**). At acidic condition, the protonation of tertiary amine groups triggered the dissociation of micelles, resulting in the release of DOX and SQ simultaneously. The DOX release profile from polymer nanocarriers after internalization into cells were investigated by monitoring the PA signals of SQ. Since the PA signal intensity was proportional to the concentration of SQ in micelles. This procedure is simple and feasible, implying that the method is a promising candidate for evaluating the drug release profile and cancer treatment efficacy at biological condition.

Experimental

Materials

3-(Diethylamino)-1-propylamine (DEPA), 3-(Dibutylamino)- 1-propylamine (DBPA), 1,6-Hexanediol diacrylate (HDDA), pyrene and Nile Red (NR) were purchased from Aldrich Chemical Corporation. Doxorubicin hydrochloride (DOX·HCl, Beijing Huafeng United Technology Co.), Methyl PEG-NH_2 2K (Seebio Biotech, Inc.), Cell counting kit-8 assay (CCK-8, Beyotime Institute of Biothechnology, China) and LysoTracer Green DND-26 (Invitrogen Co.) were used without further purification. MCF-7 cell line was purchased from cell culture center of Institute of Basic Medical Sciences, Chinese Academy of Medical Sciences (Beijing, China). Other solvents and reagents were used as preserved.

Synthesis of copolymers

The mPEG-g-poly(amino esters) graft copolymers were typically prepared by Michael addition and all synthetic procedures were carried out under an nitrogen atmosphere. Take **P1** as an example. HDDA (0.226 g, 1 mmol), DBPA (0.117 g, 0.9 mmol), mPEG-NH_2 2K (0.200 g, 0.1 mmol) were all dissolved into 2 mL dimethyl sulfoxide (DMSO), and then bubbled over N_2 for 15 min under stirring. The mixture was allowed to react for 7 days at 50 ºC, and then the final reaction solution was dialyzed against deionized water (MWCO: 3500 Da). The polymer solution was lyophilized to obtain a pale yellow solid. Another graft copolymer was prepared with the same procedure.

Characterization of copolymers

The chemical structures of graft copolymers (**P1** and **P2** in **Table 1**) were determined by ^{1}H NMR measurements. ^{1}H NMR spectra of the graft copolymers in DMSO-d^6 were recorded on a Bruker ARX 400 MHz spectrometer operating at 400 MHz. The number average molecular weight (M_n) and the weight average molecular weight (M_w) of the graft copolymers were measured by gel permeation chromatography (GPC) equipment (Waters 1515 Isocratic HPLC pump) using a Waters 2414 refractive index as the detector. The molecular weights distributions (PDI = M_w/M_n) were also recorded on it using DMF containing 0.4% LiBr as eluent with a flow rate of 1.0 mL/min at 35 ºC. The column system was calibrated with monodispersed polystyrenes standards.

Preparation of copolymer micelles

The graft copolymer micelles were prepared using the dialysis method. The graft copolymer (6 mg) was dissolved in 1 mL of DMSO under stirring. To which 2 mL of phosphate buffer (PB, 10 mM, pH 7.4) was added under constantly stirring at a rate of 100 μL/min. The resulting solution was then dialyzed against PB (pH = 7.4) for 24 h (MWCO: 2000 Da) to form the copolymer micelles.

Particle size measurements

We observed the particle size distribution and hydrodynamic diameter of the graft copolymer micelles on a dynamic light scattering (DLS) analyzer (Zetasizer Nano ZS). The measurements were operated with a He-Ne solid state laser (638.2 nm, 173 °). The micelle dispersion (1 mg/mL, pH 7.4 PB) was passed through syringe filters (0.45 μm, Millipore) before measurements and the measurements were performed in a 1.0 mL quartz cuvette at 25 °C. Then we adjusted the pH value of the micelle dispersions to 5.0 using acetate buffer and evaluated their sizes. These results were finally analyzed with a BIC particle sizing software based on the Stokes-Einstein equation.

Transmission electron microscopy (TEM)

The morphologies of the graft copolymer micelles were obtained by TEM (Tecnai G^2 20 S-TWIN) with an acceleration voltage of 200 kV. The micelle and DOX-loaded micelle dispersions (0.2 mg/mL) were formed by dialysis method in 10 mM pH 7.4 PB buffer. The samples were prepared by dropping 10 μL of the micelle solution on a copper mesh, and then most of the liquid was dried by a filter paper after 2 min. Finally, the samples were stained with uranyl acetate solution for 40 s with the filter paper drying the spare liquid.

pH titration of copolymers

The graft copolymers were dissolved in distilled water with a final concentration of 1.0 mg/mL and the pH values were tuned to 3.0 by hydrochloric acid. The pH of the solution was adjusted to be 10.0 with a 0.1 M NaOH aqueous solution at an increment of 10 μL. The exact pH increases of the solution were monitored with a pH meter at room temperature.

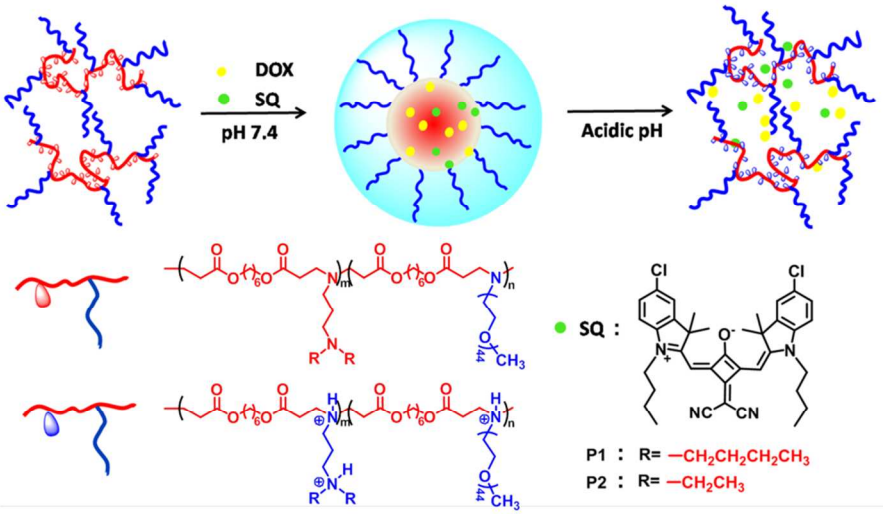

Scheme 1 DOX/SQ-Loaded micelles formation by poly(*β*-amino ester) graft copolymers and their acid-triggered dissociation of micelles for efficient DOX release

Pyrene fluorescence measurement

Pyrene was used as a hydrophobic probe to gain the fluorescence spectroscopy determining the pH sensitive properties of graft copolymer micelles. A total of 5 μL of pyrene in tetrahydrofuran (THF, 2.0×10^{-4} mol/L) was added into a 10 mL screw vial, and then THF was dried under N_2 flow. Every vial was added 5 mL of graft copolymer solutions (1.0 mg/mL) with various pH values, which were adjusted to exact pH values by PB buffer or acetate buffer. The final concentration of pyrene in each sample solution was 2.0×10^{-7} mol/L. The solution was equilibrated overnight under stirring at room temperature. A fluorescence spectrometer (F-280) was used to obtain the excitation spectra. The emission wavelength was set up at 390 nm, and the excitation spectra were recorded from 300 to 380 nm, with excitation and emission bandwidths at 5 nm. The intensity ratio of emission at 338 nm to that at 334 nm (I_{338}/I_{334}) in the excitation spectra was plotted as a function of pH values of the polymer solution.

The release of Nile Red (NR) from the micelles

The encapsulation stability and pH-dependent dissociation profiles of the graft copolymer micelles were investigated by fluorescent spectrometer using hydrophobic NR as a probe. 12 μL NR in ethanol (2.0×10^{-3} mol/L) was added into 6 mL of the micelle dispersion (1.0 mg/mL in 10 mM PB, pH 7.4). The final concentration of NR was 4.0×10^{-6} mol/L. The solution was equilibrated 8 h under stirring at room temperature before measurement on a fluorescence spectrometer (F-280) with the excitation wavelength of 545 nm. The first obtained data in pH 7.4 buffer were used as that for 0 time point. The micelle dispersion was adjusted to pH 6.8 and 5.0 by adding PB (pH 6.8, 200 mM) and acetate buffer (pH 5.0, 5.0 M), respectively, and then the fluorescence spectra of the dispersion were measured at different time intervals.

The UV-Vis spectra measurements of SQ

In order to measure the UV spectra of SQ in polymer micelles, we first prepared the SQ-loaded micelles. 60 μL SQ in DMSO (5.0×10^{-3} mol/L) was added into 6 mL of the micelle dispersion (1.0 mg/mL in 10 mM PB, pH 7.4). The final concentration of SQ was 5.0×10^{-5} mol/L. The solution was equilibrated 8 h under stirring at room temperature before measurement on a UV-Vis spectrometer (Shimadzu UV-2600, Shimadzu Co. Japan). The spectra in pH 7.4 buffer were originated from monomers. Then the micelle dispersion was adjusted to pH 5.0 by adding acetate buffer (pH 5.0, 5.0 M) to investigate the spectra of aggregated SQ. We also measured the UV-Vis spectra of free SQ at different pH values. We dissolved SQ molecules in a small amount of DMSO, and then adjusted to pH 5.5 and pH 7.4 by adding PB buffer (10 mM) before measurements.

The fluorescence spectra measurements of SQ

In order to measure the fluorescence spectra of SQ in polymer micelles, we first prepared the SQ-loaded micelles as shown above. The solution was equilibrated 8 h under stirring at room temperature before measuring on a fluorescence spectrometer (F-280) with the excitation wavelength of 670 nm. The first obtained data in pH 7.4 buffer were used as that for 0 time point. And then the micelle dispersion was adjusted to pH 6.8 and 5.0 by adding PB (pH 6.8, 200 mM) and acetate buffer (pH 5.0, 5.0 M), respectively. The fluorescence spectra of the dispersion were measured at different time intervals. The fluorescence spectra of free SQ at different pH values were measured. We dissolved SQ molecules in a small amount of DMSO, and then adjusted to pH 5.5 and pH 7.4 by adding PB buffer (10 mM). We also measured the fluorescence spectra of DOX/SQ-loaded **P1** micelles at different excitation wavelength (λ_{ex} = 475 nm, λ_{ex} = 670 nm) in PB buffer (10 mM).

PAT imaging of SQ in micelle dispersion

The SQ-loaded micelle dispersions with different SQ concentrations were added into the agarose tube (60 ºC) with the same concentration of micelles as control. After the dispersions were cooled down to the room temperature, they were scanned with PAT imaging instrument (mode: MOST 128; excitation wavelength at a range of 680-780 nm with 5 nm interval) and the PA signal was recorded through mean pixel intensity of the same area in the images. The PA signals of free SQ at different pH values were also measured. We dissolved SQ molecules in a small amount of DMSO, and then adjusted to pH 5.5 and pH 7.4 by adding PB buffer (10 mM) before measurements.

Loading of DOX in micelles

The DOX-loaded graft copolymer micelles were prepared using the dialysis method. Take DOX-loaded micelles (**Table 2**) as an example. DOX·HCl (0.60 mg) were first dissolved in DMSO (150 μL) and excessive triethylamine (DOX/TEA in molar ratio: ~1/10) was added into it to afford the hydrophobic free DOX solution. At the same time, the graft copolymer (6 mg) was dissolved in 1 mL of DMSO under stirring. 2 mL of PB (10 mM, pH 7.4) was added (100 μL/min) to the mixture of graft copolymer and free DOX solution under constantly stirring. The resulting solution was then dialyzed against PB (pH = 7.4) for 24 h (MWCO: 2000 Da) in dark to form the DOX-loaded micelles. The dispersion volume was finally set to 6 mL (1 mg/mL), and the micelles were dissolved by adding 20 μL of acetate buffer (pH 5.0, 5.0 M) to determine the DOX loading capacity and efficiency. All the measurements were performed in triplicate in the dark. DOX concentration calibration curve was obtained at 485 nm on a Shimadzu UV-2600 spectrometer in acetate buffer (pH 5.0, **Fig S6**). Then the three dissolved solution was measured at the same measurement conditions to determine the DOX loading capacity (DLC) and loading efficiency (DLE). DLC and DLE were defined as DOX in copolymer micelles/copolymer micelles (wt%) and DOX in copolymer micelles/DOX in feed (wt%), respectively.

DOX release profiles

The release profiles of DOX from pH sensitive **P1** micelles were obtained in the buffers of different pHs at 37 ºC. Briefly, 2.0 mL of the dispersed DOX-loaded micelle dispersion (1.0 mg/mL) was added to a dialysis tubing (MWCO: 10 KDa), which was then immersed in 7 mL buffer (PB for pH 7.4 and acetate for pH 5.0, 100 mM) with shaking rate at 150 rpm. At the specific time points, 0.5 mL of the dialysis solution was taken out for the UV-Vis measurement (485 nm) and replenished with 0.5 mL fresh buffer. All the measurements were performed in triplicate in the dark.

PAT imaging of SQ in cells

MCF-7 cells were grown in DMEM containing 10% FBS and 1% penicillin–streptomycin in a humidified atmosphere with 5% CO_2. The cells with a density of 7×10^6 were seeded in a 10 cm dish and incubated for different time (10 min, 30 min, 1 h, 2 h, 4 h, and 8 h) with 5 μM DOX/SQ-loaded micelles and free SQ at 37 ºC. Subsequently, the cells were washed with cold PBS three times and then harvested by trypsin. 7×10^6 cells in PBS of each time interval were mixed 1:1 with 1% ultrapure agarose (60 ºC), and then were added to the wells of agarose gel photon made in advance. The samples were scanned with PAT imaging instrument with the excitation wavelength at a range of 680-780 nm with 5 nm interval.

Confocal laser scanning microscopy (CLSM) observation

CLSM was employed to observe endocytosis and release process of DOX. A density of 5×10^5 MCF-7 cells were seeded in the 15 cm culture dishes in DMEM containing 10% FBS and 1% penicillin–streptomycin in a humidified atmosphere with 5% CO_2. The cells were first cultured with DOX-loaded graft polymer micelles for 10 min, 30 min, 1 h, 3 h, respectively, and then washed with PBS three times. The cells were incubated with LysoTracker Green DND-26 (10 μM) for 30 minutes, and then the cells were washed with cold PBS to remove the excess fluorescent dye. The cells were imaged using a Zeiss LSM710 CLSM with a 60×objective lens. For quantity analysis, the background intensity was subtracted from images before analysis.

Cytotoxicity assay

MCF-7 cells were used to determine cytotoxicity of DOX-loaded **P1** micelles by the CCK-8 assay. Free DOX, free **P1** micelles, DOX-loaded **P1** micelles (**Table 2**), SQ-loaded **P1** micelles, SQ and DOX-loaded **P1** micelles were dispersed in PB (10 mM, pH 7.4) with different concentrations. A density of 2×10^4 cells per well were seeded in the 96-well plates in DMEM containing 10% FBS and 1% penicillin–streptomycin in a humidified atmosphere with 5% CO_2 and then cultured at 37 ºC for 24 h. Different concentrations of the sample solutions were added to each well. After additional 24 h of incubation, 10 μL of CCK-8 solutions was added to each well and cultured for another 4 h. The absorbance of each sample well (A_{sample}) and control well (without drug and graft copolymer) ($A_{control}$) was measured using a Microplate reader at a test wavelength of 450 nm and a reference wavelength of 690 nm, respectively. Cell viability (%) was equal to ($A_{sample}/A_{control}$) x 100. Experiments were performed in triplicate.

Results and discussion

Synthesis of graft copolymers

In this work, in order to construct appropriate pH-sensitive graft copolymers to form micelles, we copolymerized HDDA (1.0 equiv), DBPA (0.9 equiv)/DEPA (0.9 equiv) with mPEG-NH_2 (2K) (0.1 equiv) to synthesize two amphiphilic graft copolymers (**P1**/**P2**) *via* Michael addition (**Scheme 2** and **Table 1**). The reaction temperature was 50 ºC and the reaction lasted for 7 days. ^{1}H NMR and GPC

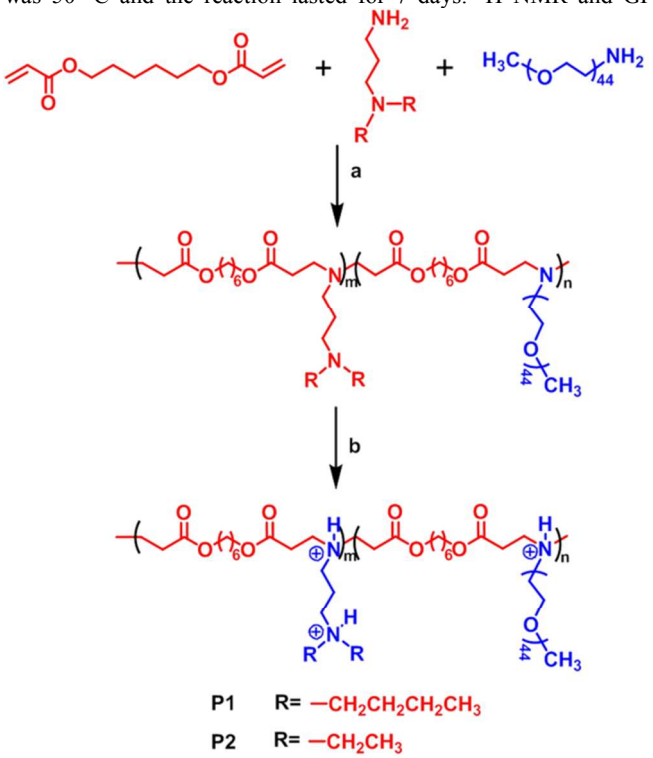

Scheme 2 Synthesis and acid-triggered protonation of the poly(*β*-amino ester)s graft copolymers. (a) DMSO, 50 ºC, 7 d. (b) H_2O/H^+

Table 1 Characterization and aggregation properties of the graft copolymers[a]

Polymer	HDDA: DBPA: DEPA: mPEG-NH_2 (2K)[b]	M_n[c]	PDI[c]	D_{h1} (nm)[d]	D_{h2} (nm)[e]	D_{h3} (nm)[f]
P1	1.0:0.9:0:0.1	17400	1.07	43.94	6.02	42.83
P2	1.0:0:0.9:0.1	19400	1.07	90.38	21.05	626.3 (2.6%) 118.5 (97.4%)

[a] Copolymerization conditions: Michael addition, DMSO, 7 d, 50 ºC. [b] Molar feed ratio. [c] Number-averaged molecular weight and polydispersity index determined by GPC with DMF as an eluent and monodispersed polystyrenes as the standards. [d] Hydrodynamic diameter measured by DLS for the graft copolymer micelle dispersions (1.0 mg/mL, pH 7.4, 10 mM PB). [e] Hydrodynamic diameter measured by DLS for the copolymer micelle dispersions (1.0 mg/mL, pH 5.0, 50 mM acetate buffer solution). [f] Hydrodynamic diameter measured by DLS for the copolymer micelle dispersions (1.0 mg/mL, pH 7.4, 10 mM PB) after 18 h.

measurements were applied to determine the structures and molecular weight of **P1** and **P2**. ^{1}H NMR showed the defined structure (**Fig 1** and **Fig S1**). The polymer units and the average number molecular weight of **P1** could also be calculated by the area of peak * belonging to the end group of acrylate *via* ^{1}H NMR. The calculated polymer units and the average molecular weight of **P1** are around 30 and 20500, respectively. GPC was also used to determine its M_n of 17400, which was in accordance with the results of NMR.

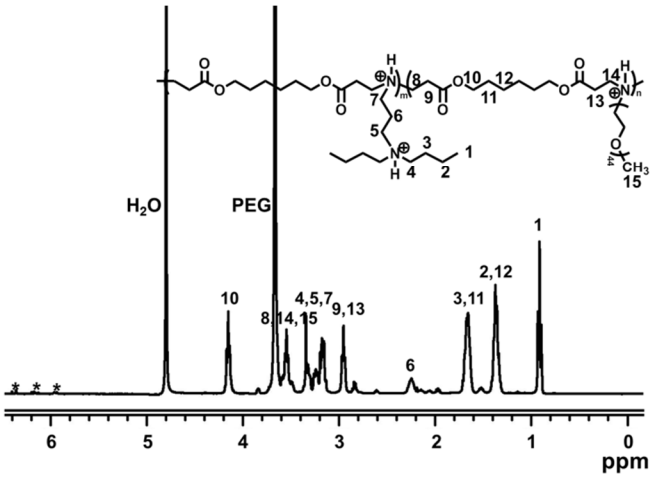

Fig. 1 ^{1}H NMR spectrum of poly(*β*-amino ester)s graft copolymers **(P1)** in D_2O containing 0.6 wt% DCl. Asterisks (*) represent the double bonds of acrylate end groups.

Formation of graft copolymer micelles

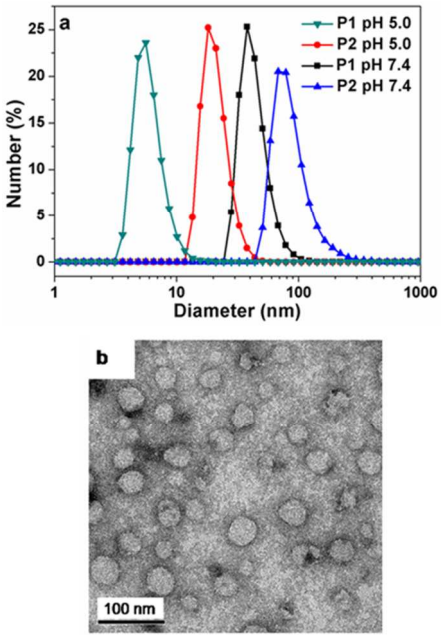

Fig. 2 (a) Number size distribution of **P1** and **P2** micelles (1.0 mg/mL) in 10 mM PB solutions (pH 7.4) and 50 mM acetate buffer (pH 5.0) measured by DLS. (b) TEM images of **P1** micelles (0.2 mg/mL) in 10 mM PB solutions at pH 7.4.

The graft copolymers **P1** and **P2** could self-assemble into micelles as described in **Scheme 1**. DBPA/DEPA and HDDA constituted the hydrophobic core while mPEG-NH_2 (2K) side chains formed the hydrophilic shell. DBPA/DEPA were also pH-sensitive with the pK_b value around 5.7 and 6.5, respectively, which was due to the different protonated degrees of the tertiary amines. According to the DLS results (**Table 1, Fig 2a**), **P1** and **P2** could both form micelles with appropriate size at pH 7.4. **P1** tended to form micelles with smaller hydrodynamic diameter (44 nm) than that of **P2 (**90 nm). We speculated that DBPA was more hydrophobic than DEPA, which caused that **P1** formed more compact micelles than **P2**. TEM micrograph showed **P1** micelles were almost spherical with an average size of 36.8±11 nm (**Fig 2b**). The size of micelle in dried state was smaller than that in aqueous solution, which could be attributed to the loss of their hydrated layers. The similar trend was also observed for **P2** micelles (**Fig S2**).

pH-Sensitive properties of graft copolymers

The poly(*β*-amino ester)s reported before exhibited pH buffering capacities. The similar buffering properties were also observed for **P1** and **P2**. As shown in the acid-base titration profiles (**Fig 3**), the buffer regions of **P1** and **P2** with various monomers were different. **P1** exhibited an obvious buffer region around pH 6.0, but **P2** displayed a broadened region of pH 4.0-9.0, which was in accordance with other copolymers with diethyl amino groups.[76] As we all know, the "proton sponge" effect of graft copolymers damage the stability of lysosomal membranes due to the protonation of tertiary amine groups. The high buffering capacity could increase endosomal escape, indicating that the graft copolymers had great potential for studying the controlled intracellular drug release behaviours.

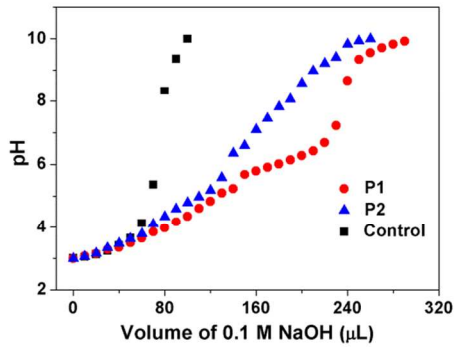

Fig. 3 Titration curve of control (NaCl aqueous solution) and graft copolymers **P1** and **P2** (1.0 mg/mL) obtained by adding 0.1 M NaOH at room temperature.

The pH sensitive properties of graft copolymer micelles were further proved by fluorescence spectroscopy using pyrene as a hydrophobic probe (**Fig S3**). The ratio of I_{338}/I_{334} could be used as an index of micelles hydrophobicity[77]. The ratio of I_{338}/I_{334} increased at pH 5.8 and 6.2 for **P1** and **P2**, respectively, implying that single polymer chains assembled into core-shell micelles above this pH. Therefore, the graft copolymers could self-assemble into micelles with hydrophobic cores at neutral pH, which dissociated in weakly acidic media.

Acid-triggered dissociation of the graft copolymer micelles

The dissociation behaviours of pH-sensitive micelles could be observed by DLS in buffers of different pHs. At pH 7.4, **P1** and **P2** formed stable micelles with size of 44 nm and 90 nm (**Table 1**), respectively. When the pH decreased to 5.0, the peaks of 6 and 21 nm were observed for **P1** and **P2**, respectively, proving that the protonation of tertiary amine groups resulted in dissociation of the micelles. Dissociation behaviours of the micelles could also be monitored by fluorescence using NR as the polarity sensitive probes. At pH 7.4 (**Fig 4a**), the emission intensity of NR did not show apparent change within 60 min, implying that NR was loaded in the **P1** micelles with high stability in this time scale. At pH 5.0, the fluorescence intensity of NR decreased sharply to ~43% within 2 min, and finally decreased to ~24% within 60 min, indicating that the micelles dissociated and hydrophobic NR was released into the aqueous solution due to the ionization of graft copolymer chains. The phenomenon corresponded with the results of DLS. At pH 6.8, the fluorescence intensity of NR decreased ~19% within 60 min, which proves that the graft copolymer micelles would be stable in tumor extracellular circumstance.

NR is also a solvatochromic dye, the maximum emission wavelength (λ_{max}) of which red-shifts as the solvent polarity increases.[78, 79] **Fig 4b** showed that λ_{max} of NR-loaded **P1** micelles was ~594 nm at pH 7.4, indicating that the NR were loaded in the hydrophobic microdomains of **P1** micelles. At pH 5.0, the emission intensity was significantly reduced and λ_{max} red-shifted to ~645 nm, we speculated that the **P1** micelles dissociated under acidic conditions, which resulted in the increased polarity of the NR microenvironment. Therefore, the graft copolymer micelles were stable in the normal physiological environment and released the drugs quickly in lysosomes (pH 5.0-6.0), indicating that micelles are promising candidates for controlled drug release.

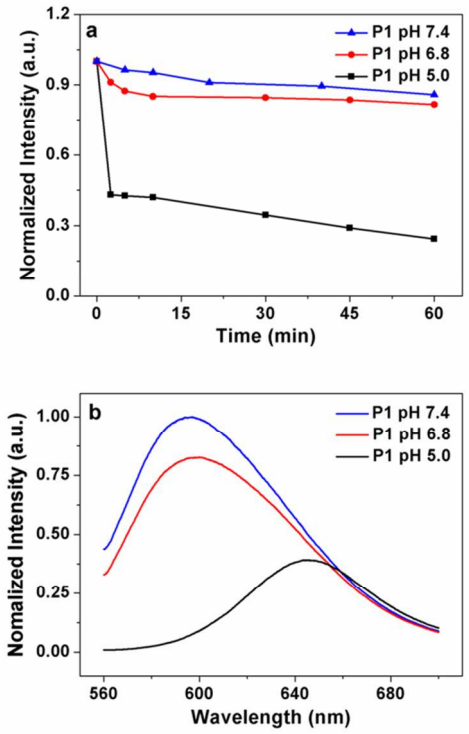

Fig. 4 (a) Incubation time-dependent change of the normalized fluorescence intensity of NR in **P1** micelle dispersions at different pHs. (b) pH-dependent fluorescence spectra of NR in **P1** micelle dispersions. λ_{ex}= 545 nm; 37 ℃ graft copolymer concentration: 1.0 mg/mL; NR concentration: 1.0×10^{-6} M.

Acid-triggered release of SQ from micelles

The release behaviours of SQ molecules in **P1** micelles at various pHs were first investigated by UV-Vis (**Fig 5a**) and fluorescence spectrometer (**Fig 5b**). The formation of SQ H-aggregates under pH 5.0 was deduced from the increased absorption ratio at 650 and 698 nm (A_{650}/A_{698}) from 0.44 to 0.79, this conclusion was consistent with our previous study.[46] The absorptions maxima at 698 nm and 650 nm corresponded with the monomer and H-aggregate bands, respectively. Moreover, the fluorescence intensity was quenched dramatically at maximum emission wavelength 721 nm with pH decrease and H-aggregate formation. The release behaviours of SQ molecules were also monitored by their changes of PA signals. Since the high noise of biological samples below the 680 nm detection wavelength, we utilized 680-780 nm with 5 nm interval as excitation wavelength to acquire PA signals of the SQ monomer encapsulated into **P1** micelles. As shown in **Fig 5c**, the similar trend was also observed for the PA signals of SQ monomer with the excitation of light pulses at 680-780 nm with 5 nm interval. We speculated that the SQ molecules were loaded in the micelles as monomer state, and then the acidic pH triggered the dissociation of micelles and aggregation of SQ molecules, resulting in the reduction of hydrophobic SQ monomers. In order to further prove that it was the aggregation of SQ molecules that led to the PA signals decreased instead of precipitation, the PA signals of SQ-loaded micelles (50 and 10 μM for SQ) with two concentrations were observed under neutral and acidic conditions. Theoretically, if SQ precipitated after the dissociation of micelles, the PA signal would drop to the same value at pH 5.0. However, with the concentration of SQ increasing, the PA signal also increased, implying that the SQ aggregated after dissociation of the micelles. We also prove that there is no obvious pH effect on UV-Vis absorbance, fluorescence and PA signals of

free SQ (**Fig S10, Fig S11**). Therefore, SQ could be potential candidates in PAT imaging and built-in reporter to monitor the drug release behaviour of the micelles.

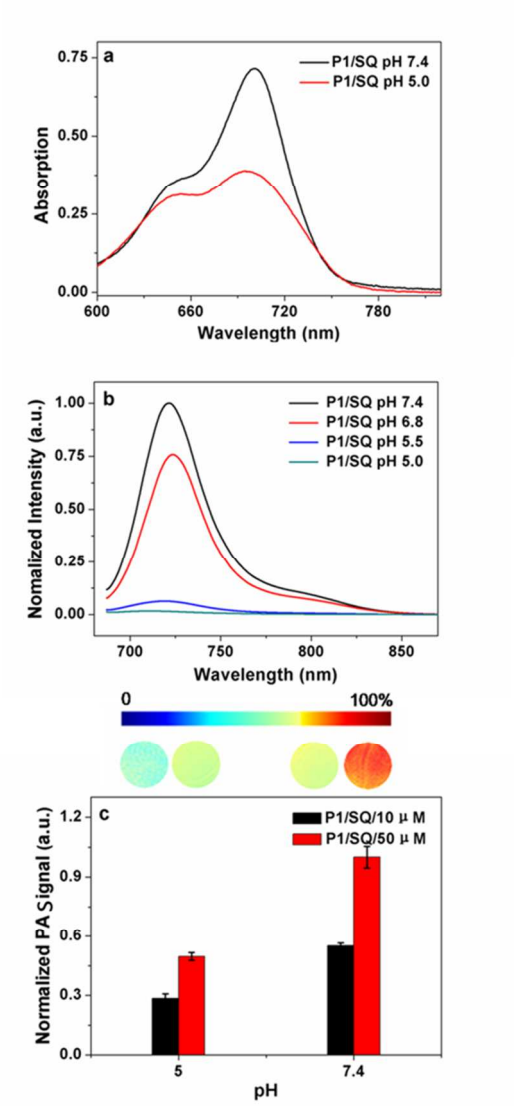

Fig. 5 (a) UV/Vis absorption of SQ-loaded **P1** micelles (50 μM) in buffer at different pHs. (b) The fluorescence intensity changes of SQ-loaded **P1** micelles (50 μM) at different pHs. (c) The PA signals changes of SQ-loaded **P1** micelles (10 μM, 50 μM) at different pHs.

The stability of SQ-loaded micelles was measured by fluorescence spectra and PAT imaging. As shown in **Fig 6a**, the fluorescence intensity of SQ at maximum emission wavelength of 721 nm did not show apparent change within 60 min at pH 7.4, while the fluorescence intensity of SQ decreased dramatically to baseline within 2 min at pH 5.0. The similar trend was observed for the PA signal of SQ (**Fig 6b**), which were in accordance with the results of NR fluorescence. The stability of encapsulated SQ is important for evaluating the process of micelle dissociation and drug release behaviour.

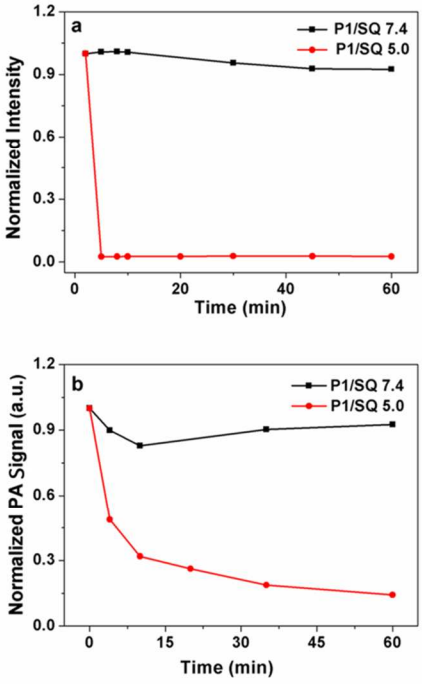

Fig. 6 (a) pH-Dependent fluorescence spectra of SQ-loaded **P1** micelle dispersions. λ_{ex} = 670 nm. (b) pH-Dependent PA signals of SQ-loaded **P1** micelle dispersions; 37 ºC; graft copolymer concentration: 1.0 mg/mL; SQ concentration: 5.0×10^{-5} M.

DOX loading and pH-dependent release

Anticancer drugs DOX were loaded in micelles by dialysis method. With the feed ratio of DOX increasing, the loading content of **P1** micelles increased while loading efficiencies decreased (**Table 2**). The results also showed that the DOX loading efficiencies were approximately 84% and 64% for **P1** and **P2** micelles at the same feed ratio (5 wt%), respectively. We speculated that the stronger hydrophobicity of DBPA resulted in the increase of DOX loading amount.

Table 2 Loading content and efficiency of DOX-loaded copolymer micelles [a]

Polymer	HDDA: DBPA: DEPA: mPEG-NH_2 (2K)	w_d/w_p (wt %)[b]	DLC (wt %)[c]	DLE (wt %)[d]
P1	1.0:0.9:0:0.1	5	4.20±0.14	84.0±2.8
P1	1.0:0.9:0:0.1	10	4.65±0.18	46.5±1.8
P2	1.0:0:0.9:0.1	5	3.70±0.18	64.0±3.6
P2	1.0:0:0.9:0.1	10	4.01±0.05	40.1±0.5

[a] Drug loading content experiments were performed in PB (10 mM, pH 7.4). [b] w_d/w_p denotes the percent drug/polymer ratio in feed, that is, the initial percent feed ratio. [c] Drug loading content (DLC) defined as the percent ratio of drug in polymer micelles/polymer micelles. [d] Drug loading efficiency (DLE) defined as the percent ratio of drug in polymer micelles/drug in feed.

The size and stability of DOX-loaded micelles played important roles in the application as drug carriers. The size of DOX-loaded micelles affected cellular uptake, stability, the EPR effect *in vivo*, etc.[80, 81] The average hydrodynamic diameters of DOX-loaded **P1**

and **P2** micelles were around 79 and 175 nm, respectively (**Fig 7**), which were higher than that of the blank micelles due to the hydrophobicity of DOX. The diameter of DOX-loaded **P1** micelle dispersions did not exhibit apparent change within 5 h at 37 ºC (**Fig S12**), indicating that DOX-loaded **P1** micelles had good incubation stability.

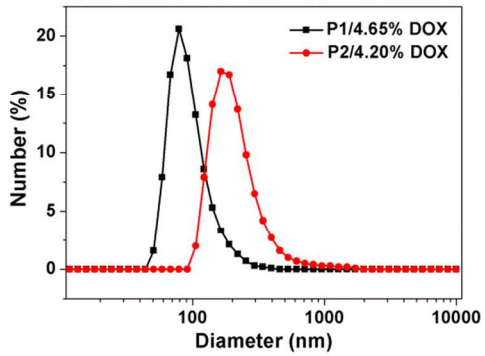

Fig. 7 Number size distribution of DOX-loaded **P1** and **P2** micelles in 10 mM PB solutions (pH 7.4) measured by DLS.

The DOX release profiles from the pH-sensitive **P1** micelles (**Table 2**) were measured by a dialysis method. The cumulative release of DOX from **P1** micelles at pH 7.4 and pH 6.8 were only 16% and 19% within 5 h (**Fig 8**), respectively, indicating that the DOX-loaded **P1** micelles could preserve stable nanostructures at physiological environment and tumor extracellular circumstance (**Fig S13**). However, at pH 5.0, significantly accelerated DOX release was observed with a ~45% release within 15 min and up to ~65% in 5 h, which was attributed to the quick dissociation of micelles. The release behaviours of DOX were in accordance with the results of DLS and NR fluorescence measurements.

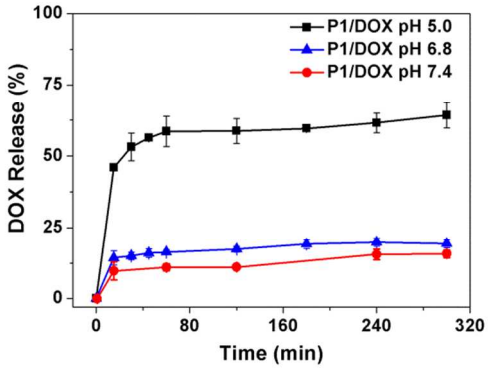

Fig. 8 *In vitro* cumulative release profiles of DOX from **P1** micelles at different pHs at 37 ºC. Graft copolymer concentration: 1.0 mg/mL.

Monitoring DOX release by PAT imaging and CLSM validation

In order to demonstrate SQ can monitor the release behaviours of DOX at the cellular level using PAT methods, we first prepared the DOX/SQ-loaded micelles. As shown in UV-Vis absorption spectra (**Fig S14**), there were two absorption peaks at wavelength 700 nm and 507 nm, which were in accordance with the SQ and DOX absorptions. Therefore, both the DOX and SQ were loaded in the **P1** micelles. As shown in **Fig S15** and **Fig S16**, we also measured the fluorescence spectra of DOX/SQ-loaded micelles at different excitation wavelength (λ_{ex} = 670 nm, λ_{ex} = 475 nm). There were no obvious optical changes (10 nm red shifted) of SQ, which have no effect on the subsequent PAT imaging. Then the cells were incubated with free SQ and DOX/SQ-loaded **P1** micelles for different time scales before PAT imaging. For the cells incubated with free SQ (**Fig S17**), with increase of incubation time, the PA signal increased gradually due to the accumulation of SQ molecules in cells. For the cells incubated with DOX/SQ-loaded **P1** micelles, with increase of incubation time, the PA signal increased gradually after 10 min and reached a maximum value at 1 h, followed by the decrease of signal to 33% eventually (**Fig 9**). We speculated that the PA signal enhanced in 1 h due to the accumulation of the DOX/SQ-loaded micelles in cells by endocytosis. Subsequently, the micelles were dissociated in lysosomes, accompanied by the release of DOX and SQ. The released SQ monomers formed H-aggregates, resulting in the decrease of PA signal. This phenomenon was different from the PA signals changes of cells incubated with free SQ. Therefore, the real-time and quantified monitoring of DOX release in biological media was realized by PAT imaging of SQ-loaded micelles.

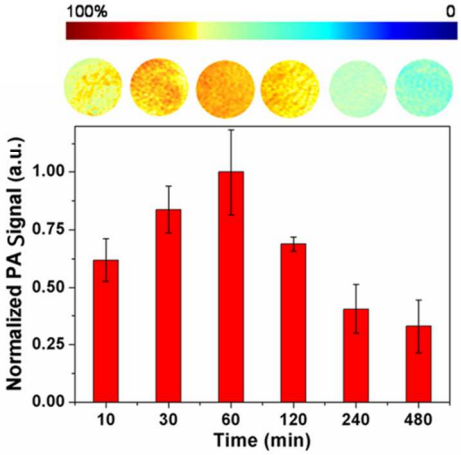

Fig. 9 PA signals changes of MCF-7 cells treated with SQ/DOX-loaded **P1** micelles for different time points at 5 μM.

CLSM was also utilized to validate the release process and subcellular biodistribution of DOX in MCF-7 cells. We have used free DOX as control in different time points (**Fig S19**). With increase of incubation time, the free DOX fluorescence intensity increased gradually due to the accumulation of DOX in the nucleus of cells. Then the cells were incubated with DOX-loaded P1 micelles at 37 ºC for 10 min, 30 min, 1 h, 3 h, respectively (DOX concentration: 5 μg/mL). The lysosomes were identified with LysoTracker Green to ensure the subcellular localization of DOX-loaded micelles. As shown in **Fig 10**, DOX signal colocalized with endosomes/lysosome in 40 min and 1 h, indicating that the DOX-loaded micelles were internalized by cellular endocytosis pathways, mainly distributed in lysosomes. At 1.5 h, the DOX fluorescence was observed in cytoplasm, implying DOX was released from micelles followed by entering the cytoplasm. At 3.5 h, larger amount of DOX was released and a part of free DOX entered into the nucleus region. The results were in accordance with the variation of PA signals, proving the feasibility of PAT imaging.

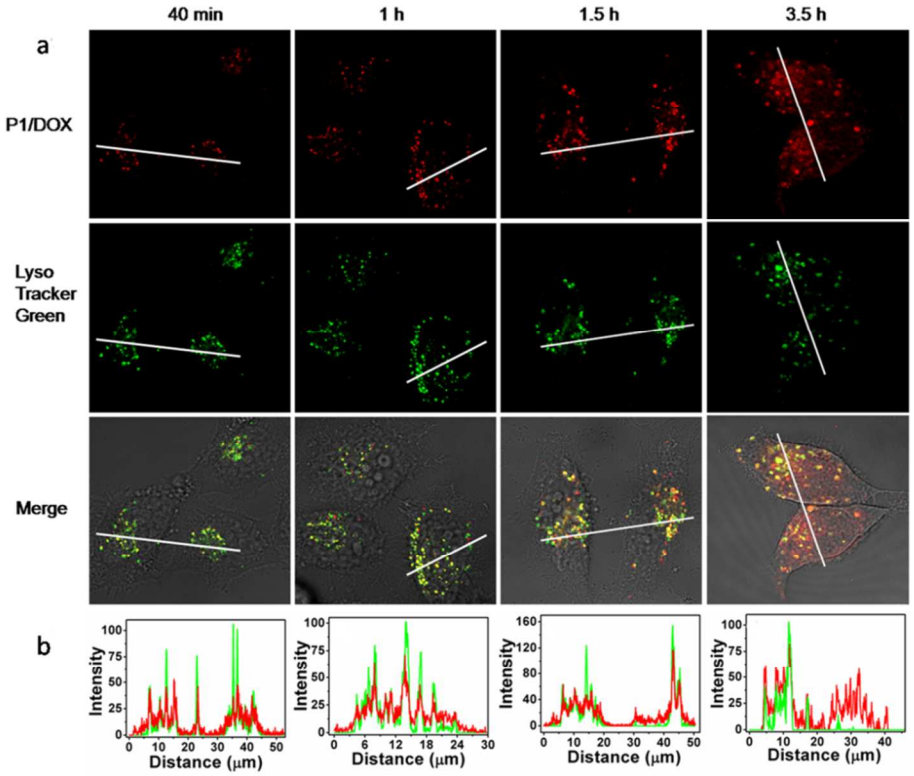

Fig. 10 (a) Confocal microscopy of living MCF-7 cells that were incubated with **P1**/DOX (5 μg/mL) for 10 min, 0.5 h, 1 h, 3 h, respectively; (b) Representative line pot of MCF-7 cells incubated with **P1**/DOX (5 μg/mL) for 40 min, 1 h, 1.5 h, 3.5 h, respectively. Lysosomes were labeled with LysoTracker Green (10 μM) for 30 min before imaging.

Cytotoxicity and cellular uptake of DOX-loaded micelles

The cytotoxicity of DOX-loaded micelles toward MCF-7 cells was carried out by CCK-8 assay using free DOX as a positive control within 24 h **(Fig 11)**. The blank micelles and SQ-loaded micelles did not show significant cytotoxicity at a concentration up to ~215 μg/mL and 50 μM, respectively. The cytotoxicity of free DOX, DOX-loaded micelles and DOX/SQ-loaded micelles increased with the increase of DOX concentration, implying that they were effective to kill the MCF-7 cancer cells. The cytotoxicity of DOX-loaded micelles and DOX/SQ-loaded micelles were almost the same, which were lower than that of free DOX. This might be due to the inefficient cellular internalization of the DOX-loaded micelles shielded by the hydrophilic PEG chains.

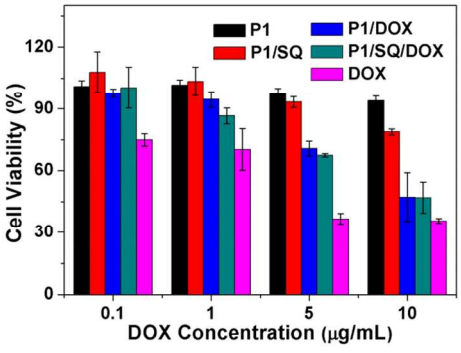

Fig. 11 MCF-7 cell viability measured by CCK-8 assay. The DOX-loaded **P1** micelles (**Table 2**) with the initial feed ratio of 10% were used for the experiments. Results are presented as the mean ± SD in triplicate.

Conclusion

We have developed a novel and facile method to evaluate the drug release profiles from drug-loaded polymer carriers using PAT imaging. The graft polymers poly(*β*-amino ester)s with PEG side chains formed micelle-like nanoparticles with hydrophobic cores, which were stable at neutral pH and dissociated into single chains at acidic condition. The micelles could load anticancer drug DOX and NIR dyes SQ simultaneously with controlled release at different pHs. The drug-loaded micelles entered lysosomes gradually in 1 h, followed by drug release from micelles into cytoplasm, which were proved by variation of PAT imaging. Therefore, PAT imaging has great potential for evaluation of controlled drug release process and anticancer efficiency in biological environment.

Conflict of interest

The authors declare no competing financial interest.

Acknowledgments

This work was supported by National Basic Research Program of China (973 Program, 2013CB932701), National Natural Science Foundation of China (21374026, 21304023, 51373046 and 51303036), Hebei Provincial Natural Science Foundation of China (B2014202209) and Beijing Natural Science Foundation (2132053) and the 100-Talent Program of the Chinese Academy of Science (Y2462911ZX). Thanks Prof. Würthner for kindly providing SQ molecules.

Appendix A. Supplementary data

More characterization of the copolymers, additional results of TEM images, fluorescence spectra, UV/Vis spectra, PAT imaging, calibration curve of DOX, and CLSM images.

References

[a] School of Chemical Engineering & Technology, Hebei University of Technology, Tianjin, 300130, China. [b] CAS Key Laboratory for Biological Effects of Nanomaterials and Nanosafety, National Center for Nanoscience and Technology (NCNST), Beijing, 100190, China.
Email: wanghao@nanoctr.cn or E-mail: zyduan@hebut.edu.cn
Homepage: http://www.nanoctr.cn/wanghao

1. Y. Zhao, F. Sakai, L. Su, Y. Liu, K. Wei, G. Chen and M. Jiang, *Adv. Mater.*, 2013, **25**, 5215-5256.
2. Y. Liu, Z. Wang and X. Zhang, *Chem. Soc. Rev.*, 2012, **41**, 5922-5932.
3. O. C. Farokhzad and R. Langer, *ACS Nano*, 2009, **3**, 16-20.
4. H. Lu, J. Wang, Z. Song, L. Yin, Y. Zhang, H. Tang, C. Tu, Y. Lin and J. Cheng, *Chem. Commun.*, 2014, **50**, 139-155.
5. K. Kataoka, A. Harada and Y. Nagasaki, *Adv. Drug Delivery Rev.*, 2001, **47**, 113-131.
6. R. Haag and F. Kratz, *Angew. Chem., Int. Ed.*, 2006, **45**, 1198-1215.
7. A. Sionkowska, *Prog. Polym. Sci.*, 2011, **36**, 1254-1276.
8. J. H. Park, S. Lee, J.-H. Kim, K. Park, K. Kim and I. C. Kwon, *Prog. Polym. Sci.*, 2008, **33**, 113-137.
9. A. Vashist, A. Vashist, Y. K. Gupta and S. Ahmad, *J. Mater. Chem. B,* 2014, **2**, 147-166.
10. T. Krasia-Christoforou and T. K. Georgiou, *J. Mater. Chem. B*, 2013, **1**, 3002-3025.
11. J. S. Lee and J. Feijen, *J. Controlled Release*, 2012, **161**, 473-483.
12. L. Brannon-Peppas and J. O. Blanchette, *Adv. Drug Delivery Rev.*, 2004, **56**, 1649-1659.
13. A. S. Mikhail and C. Allen, *J. Controlled Release*, 2009, **138**, 214-223.
14. L. Wang, L.-l. Li, Y.-s. Fan and H. Wang, *Adv. Mater.*, 2013, **25**, 3888-3898.
15. J.-H. Xu, F.-P. Gao, X.-F. Liu, Q. Zeng, S.-S. Guo, Z.-Y. Tang, X.-Z. Zhao and H. Wang, *Chem. Commun.*, 2013, **49**, 4462-4464.
16. L. Wang, L.-L. Li, H. L. Ma and H. Wang, *Chin. Chem. Lett.*, 2013, **24**, 351-358.
17. J. Siepmann and N. A. Peppas, *Adv. Drug Delivery Rev.*, 2012, **64**, 163-174.
18. N. Ahuja, O. P. Katare and B. Singh, *Eur. J. Pharm. Biopharm.*, 2007, **65**, 26-38.
19. J. Ko, K. Park, Y. S. Kim, M. S. Kim, J. K. Han, K. Kim, R. W. Park, I. S. Kim, H. K. Song, D. S. Lee and I. C. Kwon, *J. Controlled Release*, 2007, **123**, 109-115.
20. J. Chen, X. Qiu, J. Ouyang, J. Kong, W. Zhong and M. M. Q. Xing, *Biomacromolecules*, 2011, **12**, 3601-3611.
21. W. Song, Z. Tang, M. Li, S. Lv, H. Yu, L. Ma, X. Zhuang, Y. Huang and X. Chen, *Macromol. Biosci.*, 2012, **12**, 1375-1383.
22. M. Xu and L. V. Wang, *Rev. Sci. Instrum.*, 2006, **77**, 041101.
23. L. V. Wang and S. Hu, *Science*, 2012, **335**, 1458-1462.
24. V. Ntziachristos and D. Razansky, *Chem. Rev.*, 2010, **110**, 2783-2794.
25. Z. Liu, S. Tabakman, K. Welsher and H. Dai, *Nano Res.*, 2009, **2**, 85-120.
26. A. De la Zerda, C. Zavaleta, S. Keren, S. Vaithilingam, S. Bodapati, Z. Liu, J. Levi, B. R. Smith, T. J. Ma, O. Oralkan, Z. Cheng, X. Chen, H. Dai, B. T. Khuri-Yakub and S. S. Gambhir, *Nat. Nanotechnol.*, 2008, **3**, 557-562.
27. X.-D. Li, X.-L. Liang, X.-L. Yue, J.-R. Wang, C.-H. Li, Z.-J. Deng, L.-J. Jing, L. Lin, E.-Z. Qu, S.-M. Wang, C.-L. Wu, H.-X. Wu and Z.-F. Dai, *J. Mater. Chem. B*, 2014, **2**, 217-223.
28. Q. Zhang, N. Iwakuma, P. Sharma, B. M. Moudgil, C. Wu, J. McNeill, H. Jiang and S. R. Grobmyer, *Nanotechnology*, 2009, **20**, 395102.
29. J.-W. Kim, E. I. Galanzha, E. V. Shashkov, H.-M. Moon and V. P. Zharov, *Nat. Nanotechnol.*, 2009, **4**, 688-694.
30. A. Dragulescu-Andrasi, S. R. Kothapalli, G. A. Tikhomirov, J. Rao and S. S. Gambhir, *J. Am. Chem. Soc.*, 2013, **135**, 11015-11022.
31. E. Huynh, J. F. Lovell, B. L. Helfield, M. Jeon, C. Kim, D. E. Goertz, B. C. Wilson and G. Zheng, *J. Am. Chem. Soc.*, 2012, **134**, 16464-16467.
32. J. Levi, S. R. Kothapalli, T.-J. Ma, K. Hartman, B. T. Khuri-Yakub and S. S. Gambhir, *J. Am. Chem. Soc.*, 2010, **132**, 11264-11269.
33. J. F. Lovell, C. S. Jin, E. Huynh, H. Jin, C. Kim, J. L. Rubinstein, W. C. W. Chan, W. Cao, L. V. Wang and G. Zheng, *Nat. Mater.*, 2011, **10**, 324-332.
34. U. Mayerhoeffer, B. Fimmel and F. Würthner, *Angew. Chem., Int. Ed.*, 2012, **51**, 164-167.
35. J. M. Baumes, J. J. Gassensmith, J. Giblin, J.-J. Lee, A. G. White, W. J. Culligan, W. M. Leevy, M. Kuno and B. D. Smith, *Nature Chem.*, 2010, **2**, 1025-1030.
36. J.-J. Lee, A. G. White, J. M. Baumes and B. D. Smith, *Chem. Commun.*, 2010, **46**, 1068-1069.
37. J. R. Johnson, N. Fu, E. Arunkumar, W. M. Leevy, S. T. Gammon, D. Piwnica-Worms and B. D. Smith, *Angew. Chem., Int. Ed.*, 2007, **46**, 5528-5531.
38. J. J. Gassensmith, J. M. Baumes and B. D. Smith, *Chem. Commun.*, 2009, 6329-6338.
39. U. Mayerhoeffer, M. Gsaenger, M. Stolte, B. Fimmel and F. Würthner, *Chem. Eur. J.*, 2013, **19**, 218-232.
40. D. Ramaiah, I. Eckert, K. T. Arun, L. Weidenfeller and B. Epe, *Photochem. Photobiol.*, 2004, **79**, 99-104.
41. D. Ramaiah, I. Eckert, K. T. Arun, L. Weidenfeller and B. Epe, *Photochem. Photobiol.*, 2002, **76**, 672-677.
42. S. Sreejith, P. Carol, P. Chithra and A. Ajayaghosh, *J. Mater. Chem.*, 2008, **18**, 264-274.
43. U. Mayerhoeffer, K. Deing, K. Gruss, H. Braunschweig, K. Meerholz and F. Würthner, *Angew. Chem., Int. Ed.*, 2009, **48**, 8776-8779.
44. H. Wang, T. E. Kaiser, S. Uemura and F. Würthner, *Chem. Commun.*, 2008, 1181-1183.
45. T. Heek, F. Würthner and R. Haag, *Chem-a. Eur. J.*, 2013, **19**, 10911-10921.

46. F. P. Gao, Y. X. Lin, L. L. Li, Y. Liu, U. Mayerhoffer, P. Spenst, J. G. Su, J. Y. Li, F. Wurthner and H. Wang, *Biomaterials*, 2014, **35**, 1004-1014.
47. K. Ulbrich, *Adv. Drug Delivery Rev.*, 2004, **56**, 1023-1050.
48. C. J. F. Rijcken, O. Soga, W. E. Hennink and C. F. van Nostrum, *J. Controlled Release*, 2007, **120**, 131-148.
49. F. H. Meng, Z. Y. Zhong and J. Feijen, *Biomacromolecules*, 2009, **10**, 197-209.
50. E. S. Lee, K. T. Oh, D. Kim, Y. S. Youn and Y. H. Bae, *J. Controlled Release*, 2007, **123**, 19-26.
51. H. Q. Yin, E. S. Lee, D. Kim, K. H. Lee, K. T. Oh and Y. H. Bae, *J. Controlled Release*, 2008, **126**, 130-138.
52. S. Y. Park, H. J. Baik, Y. T. Oh, K. T. Oh, Y. S. Youn and E. S. Lee, *Angew. Chem., Int. Ed.*, 2011, **50**, 1644-1647.
53. E. M. Bachelder, T. T. Beaudette, K. E. Broaders, J. Dashe and J. M. J. Frechet, *J. Am. Chem. Soc.*, 2008, **130**, 10494-10495.
54. E. R. Gillies, T. B. Jonsson and J. M. J. Frechet, *J. Am. Chem. Soc.*, 2004, **126**, 11936-11943.
55. N. Murthy, Y. X. Thng, S. Schuck, M. C. Xu and J. M. J. Frechet, *J. Am. Chem. Soc.*, 2002, **124**, 12398-12399.
56. W. Chen, F. H. Meng, R. Cheng and Z. Y. Zhong, *J. Controlled Release*, 2010, **142**, 40-46.
57. J. Heller and J. Barr, *Biomacromolecules*, 2004, **5**, 1625-1632.
58. X. N. Huang, F. S. Du, R. Ju and Z. C. Li, *Macromol. Rapid. Commun.*, 2007, **28**, 597-603.
59. Z.-Y. Qiao, R. Ji, X.-N. Huang, F.-S. Du, R. Zhang, D.-H. Liang and Z.-C. Li, *Biomacromolecules*, 2013, **14**, 1555-1563.
60. Z. Y. Qiao, R. Zhang, F. S. Du, D. H. Liang and Z. C. Li, *J. Controlled Release*, 2011, **152**, 57-66.
61. Z. Y. Qiao, F. S. Du, R. Zhang, D. H. Liang and Z. C. Li, *Macromolecules*, 2010, **43**, 6485-6494.
62. Z.-Y. Qiao, J. Cheng, R. Ji, F.-S. Du, D.-H. Liang, S.-P. Ji and Z.-C. Li, *RSC Adv.*, 2013, **3**, 24345-24353.
63. C.-C. Song, C.-C. Su, J. Cheng, F.-S. Du, D.-H. Liang and Z.-C. Li, *Macromolecules*, 2013, **46**, 1093-1100.
64. P. Chytil, T. Etrych, C. Konak, M. Sirova, T. Mrkvan, J. Boucek, B. Rihova and K. Ulbrich, *J. Controlled Release*, 2008, **127**, 121-130.
65. Y. Bae, A. W. G. Alani, N. C. Rockich, T. S. Z. C. Lai and G. S. Kwon, *Pharm. Res.*, 2010, **27**, 2421-2432.
66. S. Lee, K. Saito, H.-R. Lee, M. J. Lee, Y. Shibasaki, Y. Oishi and B.-S. Kim, *Biomacromolecules*, 2012, **13**, 1190-1196.
67. W. She, K. Luo, C. Zhang, G. Wang, Y. Geng, L. Li, B. He and Z. Gu, *Biomaterials*, 2013, **34**, 1613-1623.
68. S. Aryal, C.-M. J. Hu and L. Zhang, *ACS Nano*, 2009, **4**, 251-258.
69. L. Meng, W. Huang, D. Wang, X. Huang, X. Zhu and D. Yan, *Biomacromolecules*, 2013, **14**, 2601-2610.
70. H. Devalapally, D. Shenoy, S. Little, R. Langer and M. Amiji, *Cancer Chemoth. Pharm.*, 2007, **59**, 477-484.
71. D. Shenoy, S. Little, R. Langer and M. Amiji, *Mol. Pharm.*, 2005, **2**, 357-366.
72. A. Akinc, D. M. Lynn, D. G. Anderson and R. Langer, *J. Am. Chem. Soc.*, 2003, **125**, 5316-5323.
73. D. M. Lynn, M. M. Amiji and R. Langer, *Angew. Chem., Int. Ed.*, 2001, **40**, 1707-1710.
74. D. M. Lynn and R. Langer, *J. Am. Chem. Soc.*, 2000, **122**, 10761-10768.
75. Z. Y. Qiao, S. L. Qiao, G. Fan, Y. S. Fan, Y. Chen and H. Wang, *Polym. Chem.*, 2014, **5**, 844-853.
76. K. Zhou, Y. Wang, X. Huang, K. Luby-Phelps, B. D. Sumer and J. Gao, *Angew. Chem., Int. Ed.*, 2011, **50**, 6109-6114.
77. F. M. Winnik, *Chem. Rev.*, 1993, **93**, 587-614.
78. J. W. Weiss, J. and A. Laschewsky, *Langmuir*, 2011, **27**, 4465-4473.
79. O. A. Kucherak, S. Oncul, Z. Darwich, D. A. Yushchenko, Y. Arntz, P. Didier, Y. Mély and A. S. Klymchenko, *J. Am. Chem. Soc.*, 2010, **132**, 4907-4916.
80. M. E. Davis, Z. Chen and D. M. Shin, *Nat. Rev. Drug Discov.*, 2008, **7**, 771-782.
81. J. J. Green, R. Langer and D. G. Anderson, *Acc. Chem. Res.*, 2008, **41**, 749-759.